




Article

Determining Rock Joint Peak Shear Strength Based on GA-BP Neural Network Method

Chuangwei Zhu ¹, Baohua Guo ^{1,2,*} , Zhezhe Zhang ¹, Pengbo Zhong ¹, He Lu ¹  and Anthony Sigama ¹ 

¹ School of Energy Science and Engineering, Henan Polytechnic University, Jiaozuo 454000, China; 19103948962@163.com (C.Z.); zhe991027@163.com (Z.Z.); zhongpb04@163.com (P.Z.); 18567030180@163.com (H.L.); anthonymsigama@gmail.com (A.S.)

² Synergism Innovative Center of Coal Safety Production in Henan Province, Jiaozuo 454000, China

* Correspondence: guobaohua@139.com

Abstract: The peak shear strength of a rock joint is an important indicator in rock engineering, such as mining and sloping. Therefore, direct shear tests were conducted using an RDS-200 rock direct shear apparatus, and the related data such as normal stress, roughness, size, normal loading rate, basic friction angle, and JCS were collected. A peak shear strength prediction model for rock joints was established, by which a predicted rock joint peak shear strength can be obtained by inputting the influencing factors. Firstly, the study used the correlation analysis method to find out the correlation coefficient between the above factors and rock joint peak shear strength to provide a reference for factor selection of the peak shear strength prediction model. Then, the JRC-JCS model and four established GA-BP neural network models were studied to identify the most valuable rock joint peak shear strength prediction method. The GA-BP neural network models used a genetic algorithm to optimize the BP neural network with different input factors to predict rock joint peak shear strength, after dividing the selected data into 80% training set and 20% test set. The results show that the error of the JRC-JCS model is a little bigger, with a value of 11.2%, while the errors of the established GA-BP neural network models are smaller than 6%, which indicates that the four established GA-BP neural network models can well fit the relationship between the peak shear strength and selected input factors. Additionally, increasing the factor number of the input layer can effectively improve the prediction accuracy of the GA-BP neural network models, and the prediction accuracy of the GA-BP neural network models will be higher if factors that have higher correlation with the output results are used as input factors.

Keywords: rock joint; peak shear strength; JRC-JCS model; genetic algorithm; BP neural network



Citation: Zhu, C.; Guo, B.; Zhang, Z.; Zhong, P.; Lu, H.; Sigama, A. Determining Rock Joint Peak Shear Strength Based on GA-BP Neural Network Method. *Appl. Sci.* **2024**, *14*, 9566. <https://doi.org/10.3390/app14209566>

Academic Editors: Giuseppe Lacidogna and Marek Lefik

Received: 13 August 2024

Revised: 5 October 2024

Accepted: 18 October 2024

Published: 20 October 2024



Copyright: © 2024 by the authors. Licensee MDPI, Basel, Switzerland. This article is an open access article distributed under the terms and conditions of the Creative Commons Attribution (CC BY) license (<https://creativecommons.org/licenses/by/4.0/>).

1. Introduction

There are many joints in natural rock, and the failure of rock formations has a strong relationship with the strength of rock joints. The shear strength of rock joints is an important indicator in practical rock engineering such as mining, sloping, tunneling and so on. In practical engineering, when the shear strength of the rock joint needs to be established, it must be sampled on-site and is obtained only after a lot of shear tests in the lab or on-site. This process takes a lot of time and manpower to complete. Therefore, if a rock joint shear strength prediction model is established by using existing test data, the estimated rock joint shear strength can be obtained by inputting some related factors, which can save a lot of resources. The factors related to rock joint strength are mainly divided into two types. On the one hand, there are the physical factors of the rock specimen itself, such as uniaxial compressive strength, size, rock joint roughness, basic friction angle, etc. On the other hand, there are the factors related to the shearing instrument during the shearing process, such as normal stress, normal loading rate, etc. Some scholars have conducted extensive research on the relationship between the above factors and rock joint shear strength.

Through a large number of laboratory experiments and field observations, Barton first proposed a quantitative description of the joint roughness factor which was the joint roughness coefficient, or JRC, and a peak shear strength model about incorporating σ_n , φ , JRC and JCS was established [1]. Heuze et al. found that the mechanical factors of a jointed rock mass have a size effect after the test [2]. Zhang Xubin et al. carried out direct shear tests on artificial rock joints with different morphologies under constant normal load (CNL) conditions, studied the contribution of different shear components to the total shear resistance, and proposed a new model to evaluate the peak shear strength of rock joints [3]. Liu et al. analyzed the influence of normal loading rate and other factors on the shear characteristics of rock joints. The results show that a higher normal loading rate will make the joints more prone to damage and deterioration, and the peak shear strength of the joints will deteriorate faster [4]. Rui Yong et al. proposed a new JRC evaluation and comparison method to overcome the shortcomings of traditional visual comparison methods based on vector similarity measures (VSMs) [5]. In order to overcome the shortcomings of the existing two-dimensional roughness factors, Liren Ban et al. proposed two factors that represent the local characteristics of the joint profile and the overall characteristics to characterize the roughness of the rock joints [6]. Ma et al. have done experimental research on the shear properties of rocks under different normal stresses. The results show that the linear relationship between normal stress and shear strength is universal [7]. Liu et al. proposed two empirical formulas to predict the peak shear strength of a rock-concrete interface by conducting direct shear tests on rock-concrete interfaces under different normal stresses [8]. Nick Barton et al. summarized JRC and provided a clear perspective for the concepts, methods, applications and trends related to its expansion. They introduced the origin and connotations of JRC, JRC-related roughness measurement, JRC estimation method, JRC-based roughness characteristics survey, JRC-based rock joint property description, JRC's influence on rock mass properties, and JRC-based rock engineering applications [9]. The above experiments show that roughness, normal stress, different roughness of the two-body interface and normal loading rate will affect the peak shear strength.

In order to predict the peak shear strength, some scholars have established a peak strength prediction formula. Grasselli et al. carried out more than 50 constant normal load direct shear tests on seven rock types. The authors also analyzed the joint surface morphologies before and after shear and developed a method to predict joint damage during shear [10]. Shen et al. established an empirical formula for evaluating the shear strength of rock joints by shear tests of regular tooth-shaped rock joints under different normal stresses [11]. Chen et al. proposed a peak shear strength model considering anisotropic characteristics by considering the fluctuation angle and fluctuation amplitude of rock mass rock joints [12]. Yang et al. proposed a new standard for the peak shear strength of rock joints by using two three-dimensional shape factors, namely, the maximum apparent inclination angle and the roughness factor [13]. Dong et al. proposed a factor to characterize the roughness of the joint surface, and proposed an empirical formula for shear strength based on three-dimensional topography factors [14]. Tian et al. carried out three-dimensional scanning tests on 39 joint specimens, proposed morphological factors to describe joint roughness, and established a peak shear strength model [15]. Liu et al. established a new peak shear strength standard through three-dimensional morphological scanning and direct shear test, compared with the JRC-JCS model and Grasselli model. The new model significantly improved the fitting effect [16]. Wang et al. further modified the three-dimensional shape factor system of the Grasselli rock joint, and obtained a prediction model that can reflect the shear mechanism of the rock joint, revealed the control effect of distribution factors on the shear resistance of the rock joint, and proposed a peak shear strength prediction model [17]. Sheng et al. proposed a new model of joint peak shear strength in the form of a negative exponent by using normal stress, tensile strength and joint roughness factors [18]. Based on the relationship between peak dilatancy angle and normal stress, joint morphology and joint deformation resistance, an empirical formula of shear strength of irregular rock joints is proposed by Cheng et al. [19]. These scholars have

established a peak shear strength prediction formula by considering the three-dimensional morphological factors, anisotropy and other factors of the rock joint. Table 1 shows the specific formulas of these papers.

Table 1. Peak shear strength models.

Barton [1]	$\tau = \sigma_n \tan[\varphi + JRC \lg(\frac{JCS}{\sigma_n})]$	(1)
Liu [8]	$\tau = \sigma_n \tan[\varphi + JRC \lg(\frac{JCS_{ab}}{\sigma_n})]$ $JCS_{ab} = xJCS_a + yJCS_b$ $y = 41.889\varphi^{-1.091}$ $x + y = 1$	(2)
Grasselli [10]	$\tau = \sigma_n \tan[\varphi(\frac{\theta^*_{max}}{c})^{1.18 \cos \beta}][1 + \exp(-\frac{\theta^*_{max} \sigma_n}{9A_0 c \sigma_t})]$	(3)
Shen [11]	$\tau = \sigma_n \cdot \tan(\varphi + k_\beta) + k_c \cdot i$	(4)
Chen [12]	$\sigma_n \tan\left\{\left\{10.725 \ln[A^\alpha (SR_v)^{1-\alpha}] + 42.202\right\} \cdot \lg\left(\frac{JCS}{\sigma_n}\right) + \varphi\right\}$	(5)
Yang [13]	$\tau = \sigma_n \tan\left(\varphi + \frac{\theta^*_{max}}{c^{0.45}} e^{-\frac{\sigma_n}{JCS} c^{0.75}}\right)$	(6)
Dong [14]	$\tau = \sigma_p \tan\left[\varphi + \frac{\arccos(1/R_s)}{(\sigma_p + 1)^m}\right]$	(7)
Tian [15]	$\tau = \sigma_n \tan\left(\varphi + \frac{160 \cdot c'^{-0.44}}{\sigma_n / \sigma_t + 2}\right)$	(8)
Liu [16]	$\tau = \sigma_n \tan\left[\varphi + (\theta^*/n)^{0.88} \cdot h \cdot e^{-\frac{\sigma_n}{\sigma_c} \cdot h^2}\right]$	(9)
Wang [17]	$\sigma_n \tan\left\{\varphi + \frac{90^\circ(1-0.0015^{1/c^*})}{2} \times [1 + \exp(-\frac{90^\circ(1-0.0015^{1/c^*})}{18} \cdot \frac{\sigma_n}{\sigma_t})]\right\}$	(10)
Sheng [18]	$\tau = \sigma_n \tan\left[\varphi + \frac{8A_0 \theta^*_{max}}{c+1} \exp(-\frac{c^{-0.351} \sigma_n}{\sigma_t})\right]$	(11)
Cheng [19]	$\tau = \sigma_n \tan\left[\varphi + \arccos(1/R_s) \cdot \frac{1}{\mu JCS + 1}\right]$	(12)

In Formula (1), τ is the peak shear strength predicted value; σ_n is the normal stress; JRC is the roughness coefficient of the rock joint; JCS is the compressive strength of the rock joint wall; φ is the basic friction angle. In Formula (2), x and y are the sharing coefficients of rock wall and concrete walls. In Formula (3), θ^* is the apparent dip; β is the dip angle; σ_t is the tensile strength; A_0 is the contact area; c is the fitting factor. In Formula (4), K_β is the correction coefficient of the comprehensive internal friction angle of the structural plane, and K_c is the correction coefficient of the comprehensive cohesion of the structural plane. In Formula (5), α is a constant with a value of 1/3, and A is the average fluctuation amplitude coefficient of the structural plane. In Formula (7), m is the topothesy. In Formula (8), C' is the factor of the distribution. In Formula (9), h is the average joint height; n is the roughness factor; σ_c is the uniaxial compressive strength. In Formula (12), μ is the Poisson ratio, R_s is the contour surface.

With the gradual popularization of machine learning, some scholars use neural networks and other methods to predict peak shear strength. Wu et al. considered the influence of joint wall strength in combination with normal stress and joint roughness, and established a neural network model [20]. Considering the complex mapping relationship between joint shear strength and influencing factors, Huang et al. proposed a prediction model of rock joint shear strength based on a back propagation (BP) neural network, which can comprehensively consider various influencing factors, including external shear test conditions and joint factors [21]. Wang et al. collected the shear experimental data of previous scholars wherein the stable topological structure was obtained by a cross-validation algorithm and optimized a BP neural network by using MBGD, Adam and RMSprop algorithms. The effects of initial undulation angle, normal stress and water content on the strength, deformation characteristics and failure mode of red sandstone joints were analyzed [22]. Shen et al. used three machine learning (ML) algorithms, support vector machine (SVM), BP neural network (BPNN) and random forest (RF), to establish regression models for predicting the peak shear strength of joints [23]. Lin et al. constructed an intelligent prediction model by optimizing a BP neural network through a genetic algorithm; they realized the construction of a quantitative mapping relationship between fractal dimension, roughness, normal pressure, friction coefficient and mechanical properties of jointed rock. They also brought

to light the formulation of an intelligent prediction method for mechanical properties of jointed rock by considering joint morphology characteristics [24]. Liu et al. collected 1080 data sets, including SH, p-wave velocity, PLS and UCS. All data sets were divided into three categories (sedimentary rock, igneous rock and metamorphic rock) according to lithology. Based on the data sets of three rock types, a combined model combining random forest and linear regression was used to predict the uniaxial compressive strength of rock [25]. Wei et al. established an artificial neural network (ANN) method to predict the uniaxial compressive strength (UCS) of sedimentary rocks by using different input factors, such as dry density, tensile strength of Brazilian splitting, and wet density [26]. These studies are listed in Table 2. There are also many machine learning methods applied to the prediction of rock strength, such as the prediction of rock strength factors by convolutional neural networks [27–30].

Table 2. Algorithm prediction model.

Reference	Method	Input Factors	Output Factors	R ²
Wu [20]	BPNN	$\sigma_{ch}/\sigma_{cs}; JRC; \sigma_n$	τ_i/τ_s	0.913
Huang [21]	BPNN	$A_0; \theta_{max}^*; \sigma_t; \sigma_n$	τ	9.66% (error)
Wang [22]	BPNN	$JRC; JCS; \sigma_n; \varphi$	τ	0.995
		$JRC; JCS/\sigma_n; \sigma_n; \varphi$		0.993
		$A_0; c; \theta_{max}^*; \sigma_t; \sigma_n; \varphi$		0.99
		$A_0; \theta_{max}^*/(c + 1); \sigma_n/\sigma_t; JCS; \sigma_n; \varphi$		0.99
Shen [23]	SVM	$\sigma_n; \varphi; \sigma_t; \theta_{max}^*/(c + 1)$	τ	0.98
	BPNN			0.97
	RF			0.98
Lin [24]	GA-BPNN	$D; R_q; \mu; \sigma_n$	τ	0.96
Liu [25]	RF-LR	$PLS; v_p; SH$	UCS	0.93
Wei [26]	ANN	$P_d; BTS; P_{wet}$	UCS	0.79

In the existing models for predicting the peak shear strength of rock joints, the main factors considered are joint roughness, uniaxial compressive strength, etc. This paper collects experimental data related to peak shear strength and uses a BP neural network optimized by a genetic algorithm to predict rock joint shear strength by considering more related factors such as specimen size, joint roughness, normal stress, normal loading rate, JCS and so on, which can give a more accurate prediction method of rock joint shear strength.

The article is structured into several key sections. The second part provides insight into the data collection process and the method employed. Following this, the third part outlines the development of the neural network model. Subsequently, the fourth part evaluates the predictive capabilities of the established neural network model, while conducting a comparative analysis with the JRC-JCS model to anticipate the factors influencing prediction model accuracy. The fifth part critically examines objective factors overlooked in the article and proposes a potential direction for future research. Lastly, the sixth part summarizes the primary conclusions drawn from the article.

2. Materials and Methods

2.1. Data Sources

The direct shear test was carried out by using the RDS-200 rock direct shear instrument developed by GCTS company (New York, NY, USA) in the in United States, as shown in Figure 1. The normal actuator and the shear actuator are controlled by the electro-hydraulic servo control system. The maximum normal and shear loads are 50 KN and 100 KN respectively, and the accuracy is 0.01 KN. The maximum shear stroke and the maximum

normal stroke are 25 mm and 24 mm, respectively, and the accuracy is 0.001 mm. A total of 205 sets of data on JRC, normal stress and size were collected. The rock types used include silty-grained marble, granite, fine-grained sandstone, coarse-grained marble and concrete.

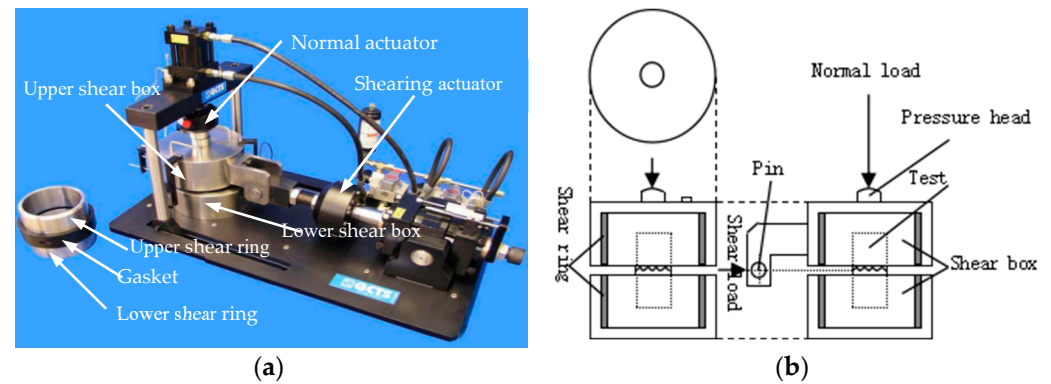


Figure 1. Schematic diagram of test device: (a) RDS-200 rock direct shear system, (b) three views of shear box.

All data are shown in Appendix A, in which the JCS is obtained by uniaxial compression test, the basic friction angle was obtained by self-tilting test, the peak shear strength τ_t is obtained from the direct shear test, the normal stress is expressed by σ_n , the basic friction angle is expressed by φ , and the normal loading rate is represented by v_n .

For the first 55 sets of data, cubic regular tooth-shaped rock-like joint specimens were used with different undulating angles and sizes prepared by high-strength sulfoaluminate cement with a water-cement ratio of 0.25. The side lengths of the square cross section of the first 30 specimens were 50 mm, 60 mm, 70 mm, 80 mm, 90 mm and 100 mm. The width of the single tooth base was 10 mm, and the fluctuation angle was 25° . The side length of the square cross-section of the next 25 specimens was 50 mm, the width of the single tooth base was 10 mm and the undulating angles were 10° , 15° , 20° , 25° and 30° . Under the condition of normal stress, the normal stresses of rock-like joint specimens were set to 2 MPa, 2.5 MPa, 3 MPa, 3.5 MPa and 4 MPa. Normal loading adopted the stress control mode, and the normal loading rate was 2 MPa/min. The shear loading was controlled by displacement, and the shear rate was 1 mm/min. The shear test process was as follows: firstly, the normal stress was applied up to the predetermined value at a loading rate of 2 MPa/min, and then the shear loading was carried out at a shear rate of 1 mm/min under the condition of keeping the normal stress constant until the shear displacement was 8 mm.

The first 55 sets of data are regular joints, as shown in Figure 2. According to the joint fractal model proposed by Xie Heping [31], the fluctuation angle of the regular rock joint is converted into JRC. The conversion formula is as follows:

$$i = \arctan\left(\frac{2h}{L}\right) \quad (13)$$

$$D = \log 4 / \log[2(1 + \cos i)] \quad (14)$$

$$JRC = 85.267(D - 1)^{0.5679} \quad (15)$$

where h is the average fluctuation difference; L is the average baseline length; i is the undulating angle; D is the fractal dimension of the rock joint, and JRC is the joint roughness coefficient.

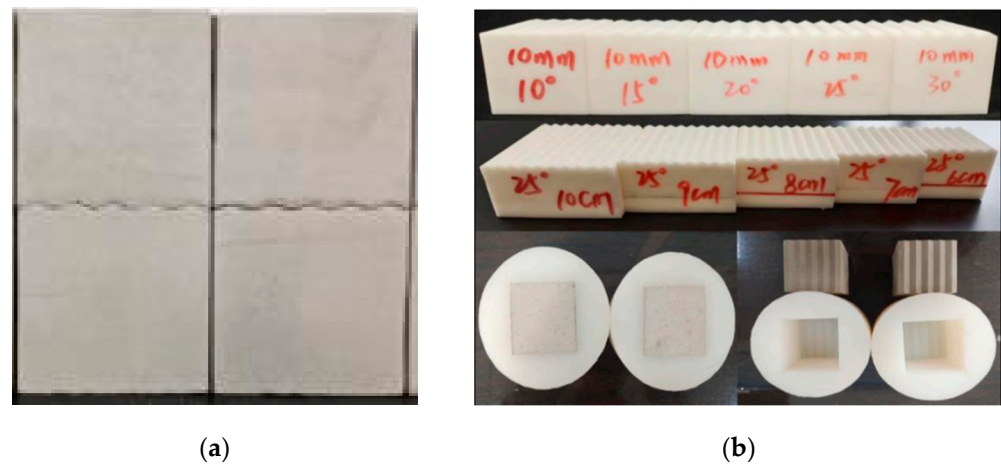


Figure 2. The first 55 sets of data: (a) specimens, (b) specimen-preparing molds.

Cylindrical rock-concrete interface specimens with a diameter of 50 mm were used to obtain the 56th to 80th sets of data. The concrete cement–sand ratio was 3.5 and the water–cement ratio was 0.32, and the samples comprised silty-grained marble-concrete interface, granite-concrete interface, fine-grained sandstone-concrete interface and coarse-grained marble-concrete interface. Direct shear tests with normal stress of 3 MPa, 4 MPa, 5 MPa, 6 MPa and 7 MPa were carried out on concrete joints and rock-concrete interfaces by using the normal stress control method with a normal loading rate of 1 MPa/min. The normal stress was then applied up to the predetermined value at a loading rate of 1 MPa/min. The shear load was applied by displacement control with a shear rate of 1 mm/min. The test was stopped when the shear displacement reached 5 mm. The joint compressive strength (JCS) of the two-body rock joint was calculated using Formula (2).

From the 56th set to the 80th set of data, the rock joint surface was scanned by a Tianyuan OKIO-400 three-dimensional scanner to obtain the joint surface morphology and extract the three-dimensional coordinate data of the profile line; the *JRC* was calculated by Formulas (16) and (17). The test specimens are shown in Figure 3.

$$Z_{2j} = \left[\frac{1}{(m-1) \Delta x^2} \sum_{i=1}^{m-1} (Z_{i+1} - Z_i)^2 \right]^{\frac{1}{2}} \quad (16)$$

$$JRC_j = 32.69 + 32.98 \lg Z_{2j} \quad (17)$$

where Z_i is the height coordinate (mm) of the i -th sampling point on the profile line; i is the sampling point serial number, a natural number; m is the total number of sampling points; Δx is the sampling interval (mm).

From set 81 to set 205, cubic rock-like joint specimens with different *JRC* and sizes were prepared using high-strength sulfoaluminate cement with a water–cement ratio of 0.25. The side lengths of the five square cross-sections were 35 mm, 50 mm, 65 mm, 80 mm and 95 mm, and the *JRCs* were 1, 5, 9, 13, and 17. The normal stress was set to 2 MPa, 2.5 MPa, 3 MPa, 3.5 MPa, and 4 MPa. The constant normal stress control method was used to apply the normal stress up to the predetermined value at a constant rate of 1 MPa/min. The shear load was applied in the shear direction by the displacement control method, and the shear load was cut at 8 mm displacement at a constant shear rate of 1 mm/min. In the process of direct shear, the normal stress was controlled constantly by the servo system. Factors such as normal stress, normal displacement, shear stress and shear displacement were recorded during the test.



Figure 3. Datasets 56 to 80: (a) joint surface, (b) specimens.

Specimen sets 81 to 205 were quantified using Barton's standard JRC profile [32]. The test specimens are shown in Figure 4.

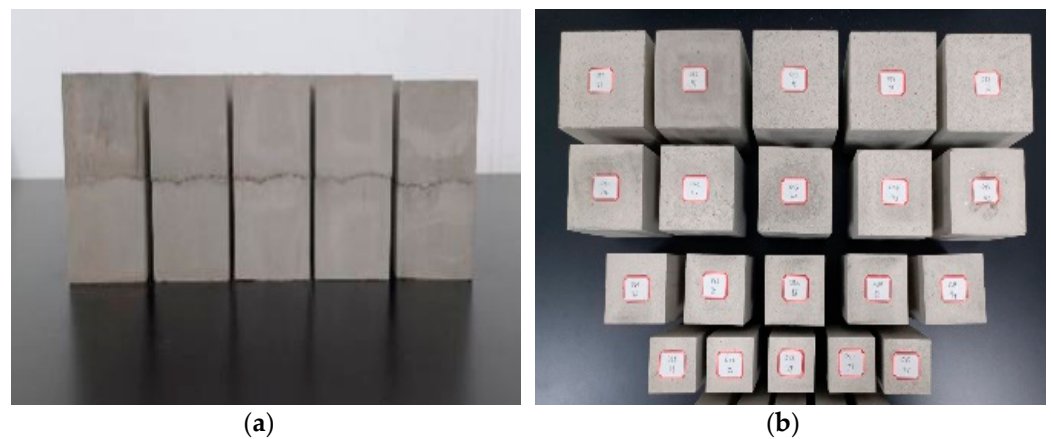


Figure 4. Datasets 81 to 205: (a) joint roughness coefficient, (b) size.

2.2. Methods

2.2.1. Correlation Analysis

The Pearson correlation coefficient was used to measure the correlation between variables. The Pearson correlation coefficient was obtained by calculating the quotient of the covariance and the standard deviation between two variables, where the covariance indicates whether the changing trend of the two variables was consistent. Standard deviation is a measure of the degree of dispersion of the variables [33]. Let two independent random variables be X and Y , and their covariances be recorded as $\text{Cov}(X, Y)$, then:

$$\text{COV}(X, Y) = E\{[X - E(X)][Y - E(X)]\} \quad (18)$$

After obtaining the covariance between two random variables X and Y , their Pearson correlation coefficients can be expressed as follows:

$$r_{XY} = \frac{\sum_{i=1}^n \text{cov}(X, Y)}{\sqrt{\sum_{k=1}^n (X_k - \bar{X})^2 \sum_{i=1}^n (Y_k - \bar{Y})^2}} \quad (19)$$

The value of the correlation coefficient r was between -1 and 1 . The greater the absolute value, the higher the correlation. The positive sign represents a positive correlation, and the negative sign represents a negative correlation.

2.2.2. Principle of GA-BP Neural Network

The BP neural network method optimized by genetic algorithm was used to predict the peak shear strength. BP neural network is a multi-layer feed-forward neural network, which is characterized by signal-forward propagation, error-back propagation, and has excellent nonlinear fitting ability and generalization ability [34]. Genetic algorithms can make it infinitely close to the global optimal solution by iteratively optimizing the calculation results [35]. Therefore, the genetic algorithm is used to optimize the initial weights and thresholds of the BP neural network model to improve the calculation efficiency and prediction accuracy of the model. The synergistic mechanism of the genetic algorithm and the BP neural network model was then constructed [36].

The BP neural network model is composed of input layer, hidden layer and output layer. Each layer contains one or more neuron nodes. Based on the multi-layer feed-forward neural network trained by the error-back propagation algorithm, the mapping relationship between the input value and the output value is established through continuous training and learning of the data [37]. The number of hidden layers is determined by Formula (20).

$$l = \sqrt{m + n} + a \quad (20)$$

where m is the number of neurons in the output layer; n is the number of neurons in the input layer; a is a constant between 1 and 12; l is the number of neurons in the hidden layer, $l \in [4, 15]$.

The constructed GA-BP neural network model is evaluated by determining coefficient (R^2), mean absolute error (MAE), mean bias error (MBE) and root mean square error (RMSE).

$$R^2 = 1 - \frac{\sum_{i=1}^n (x_{sim} - x_i)^2}{\sum_{i=1}^n (\bar{x} - x_i)^2} \quad (21)$$

$$MAE = \frac{1}{n} \sum_{i=1}^n |a_i - b_i| \quad (22)$$

$$MBE = \frac{1}{n} \sum_{i=1}^n (a_i - b_i) \quad (23)$$

$$RMSE = \sqrt{\frac{1}{n} \sum_{i=1}^n (a_i - b_i)^2} \quad (24)$$

where x_i is the experimental value; \bar{x} is the average value of the test; x_{sim} is the predicted value; a_i and b_i represent the predicted value and the actual value; n represents the number of specimens.

By calculating R^2 , the correlation between the predicted value and the real value can be observed. The higher the correlation is, the better the prediction accuracy is. The smaller the average absolute error is, the smaller the gap between the predicted value and the real value is. The closer the average deviation is to 0, the better the model fitting effect is. The trained model is used to predict the test data, and the error between the predicted value and the actual test result is observed. The accuracy of the training model is tested by the size of the error.

3. Peak Shear Strength Prediction Model

3.1. Correlation Analysis of Shear Factors

Using SPSS software (PASW Statistics 18), through the correlation analysis of various factors, the correlation between various factors and peak shear strength was discovered. Using the SPSS bivariate correlation analysis method, Pearson was used to represent the correlation coefficient, and a bilateral significance test was performed. The factors of the test

are σ_n , JRC , JCS , φ , $size$, v_n , and peak shear strength. The test results are shown in Table 3. The null hypothesis (H_0) of the Pearson correlation hypothesis test is that there is no linear relationship between the factors and the peak shear strength, and the alternative hypothesis (H_1) is that there is a linear relationship between the factors and the peak shear strength. The p -value can represent the significance level of each factor. The p -value is compared with 0.05 and 0.01. If $p > 0.05$, this indicates that the null hypothesis is established: there is no linear relationship between the selected factors and the peak shear strength. If $p \leq 0.05$, it shows that the p -value is in the rejection domain, the null hypothesis is not valid, and there is a linear relationship between the selected factors and the peak shear strength. In the range $0.01 \leq p \leq 0.05$, the significance level is higher, and “*” is used to indicate that. If $p \leq 0.01$, the significance level is very high, and “**” is used to indicate that.

Table 3. Correlation analysis between various factors and peak shear strength.

	σ	JRC	JCS	φ	$Size$	v_n
p -value	<0.01	<0.01	<0.01	<0.01	0.015	<0.01
r_{xy}	0.711 **	0.568 **	−0.309 **	0.420 **	−0.17 *	0.359 **

r_{xy} represents the relationship between the factors and the peak shear strength. It can be seen from Table 4 that the correlation coefficient between σ_n and peak shear strength is the highest, and the rest are JRC , φ , v_n , JCS , and $size$, in order of absolute value. JCS and $size$ are negatively correlated with the peak shear strength. The influence of JCS on the peak shear strength is not independent, while the correlation analysis method only considers the influence of JCS itself on the peak shear strength, without considering the normal stress, so there is a negative correlation. According to the JRC-JCS model, the correlation analysis of τ_t/σ_n and JCS/σ_n was carried out, and at $p < 0.01$, the correlation coefficient was 0.357 **.

Table 4. Evaluation of prediction results of JRC-JCS model.

R^2	MAE	MBE	RMSE
0.713497	0.458708	0.077069	0.661966

The JRC-JCS model is widely used to predict peak shear strength. The four factors contained in the model are strongly correlated with the peak shear. The calculation formula of the JRC-JCS model is given, as shown in Formula (1). The peak shear strength of rough/undulating joints such as tension surfaces can now be predicted with acceptable accuracy from a knowledge of only one factor, namely the effective joint wall compressive strength or JCS value [1].

Using the JRC-JCS model to predict 205 sets of data, the prediction results of the JRC-JCS model were obtained, and the R^2 , MAE, MBE and RMSE predicted by the JRC-JCS model were calculated, as shown in Table 4. The results calculated by the JRC-JCS model were compared with the experimental values, and the figures are shown in Figure 5.

3.2. GA-BP Neural Network

The genetic algorithm was used to optimize the BP neural network, and the GA-BP neural network peak shear strength prediction model was established. The neural network algorithm was realized by using MATLAB code. The process is shown in Figure 6. Of the 205 sets of data, 80% were used as the training set and 20% as the test set. The ratio of the training set to the test set was 4:1. The maximum number of iterations of the genetic algorithm was set to 1000, the learning rate was 0.01, the genetic generation was 50, and the population size was five. The weights and thresholds of the BP neural network can be regarded as the gene sequence in the genetic algorithm. The selection, crossover and mutation operations of the genetic algorithm were used to optimize the weights and thresholds of the neural network to achieve the effect of optimizing the neural network.

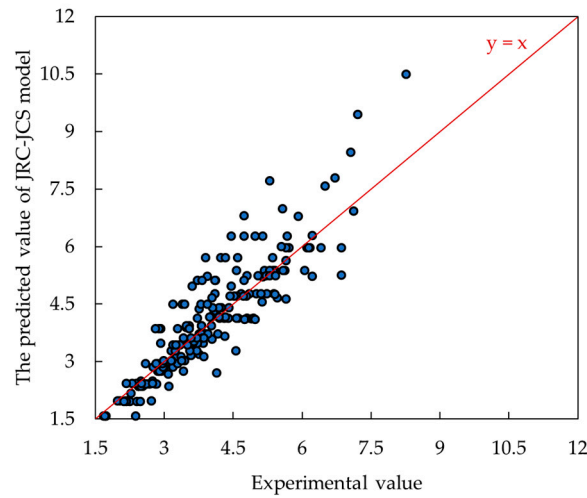


Figure 5. The scatter plot of predicted values and experimental values of the JRC-JCS model.

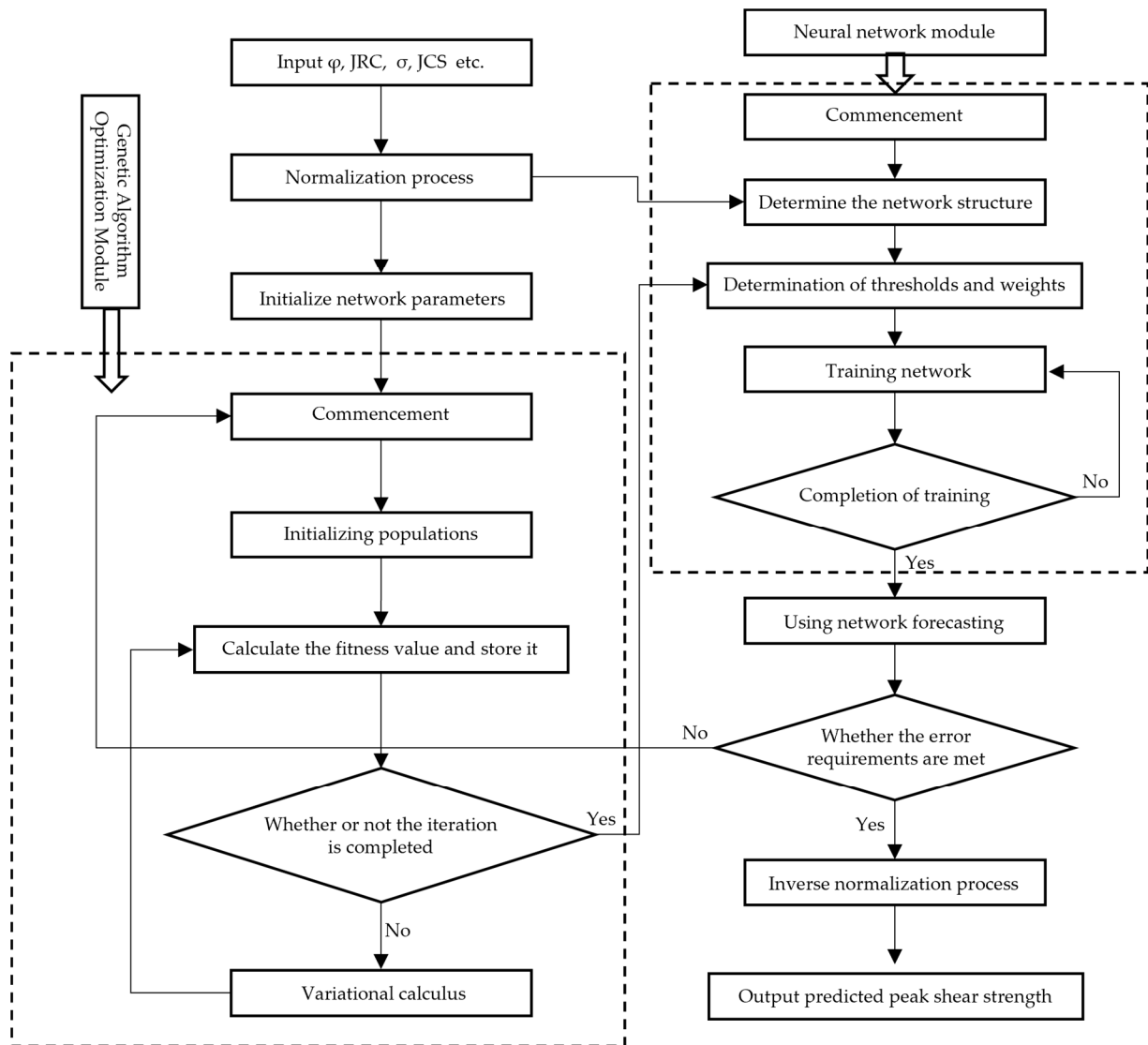


Figure 6. GA-BP neural network model prediction flow chart.

The neural network module first needs to determine the structure of the neural network. After determining the structure, the weights and thresholds obtained by the genetic

algorithm after iteration are added to the network, so that the connection between the input layer, the hidden layer and the output layer is completed. The training set data and the test set data are then used to train and test the network, so as to complete the establishment of the neural network model. Using this model, the rock joint shear strength can be predicted, and the operation can be repeated until the error requirements are met.

By observing the peak shear strength predicted by the JRC-JCS model, it can be seen that σ_n , φ , JRC , and JCS have a good mapping relationship with peak shear strength. The four factors (σ_n , φ , JRC , JCS) contained in the JRC-JCS model are used as the input layer to establish a four-factor GA-BP neural network model. The structure of the neural network is shown in Figure 7a. The input layer contains σ_n , φ , JRC , JCS , there are seven hidden layers, and the output layer is the peak shear strength.

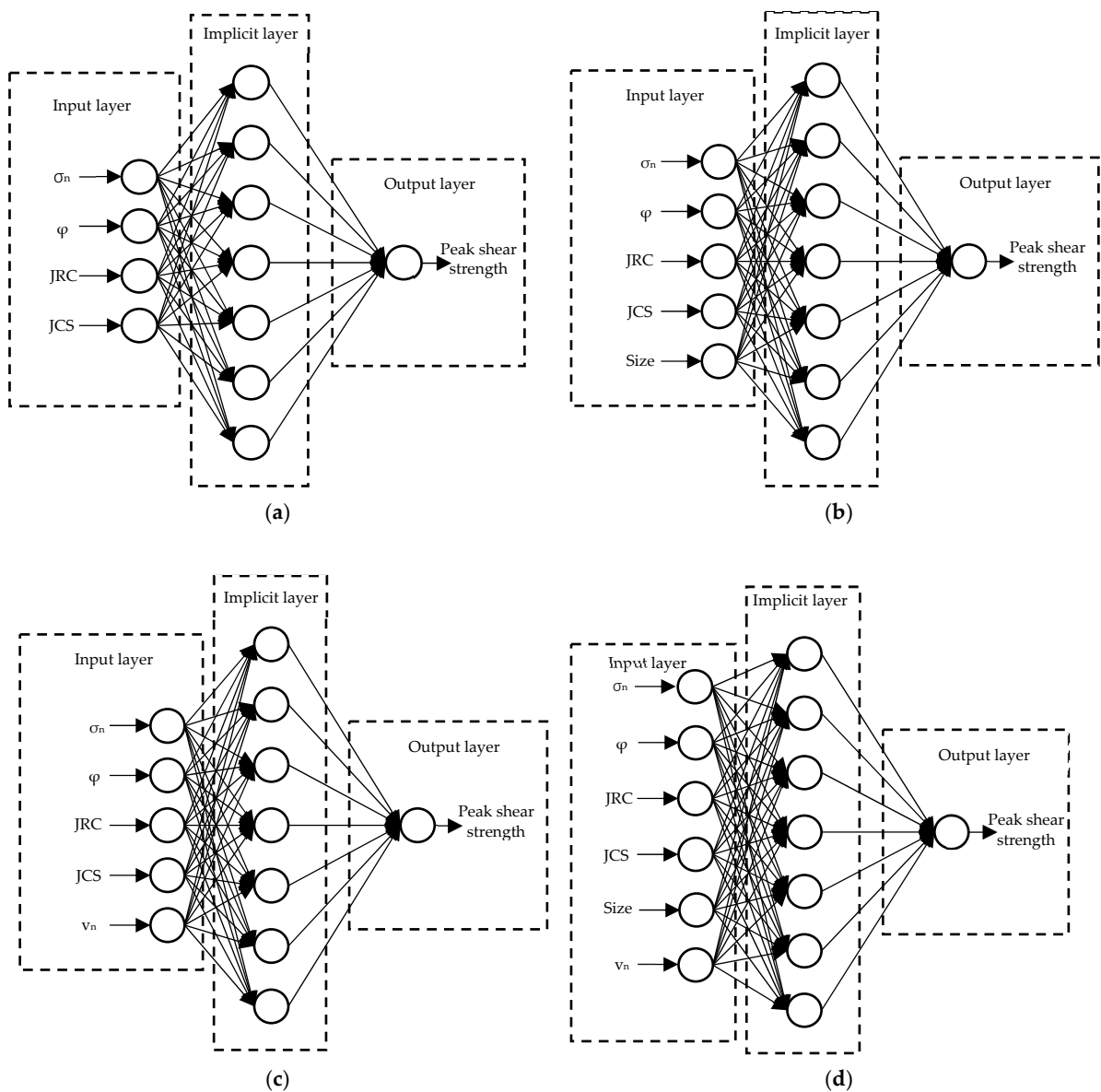


Figure 7. Neural network structure diagram: (a) GA-BP neural network four-factor model structure diagram; (b) GA-BP neural network five-factor-1 model structure diagram; (c) GA-BP neural network five-factor-2 model structure diagram; (d) GA-BP neural network six-factor model structure diagram.

Table 3 shows that in addition to the four factors of σ_n , φ , JRC and JCS , the influence of *size* and v_n on the peak shear strength is also significant. To improve the accuracy of the GA-BP neural network in predicting the peak shear strength, the factors of *size* and v_n are

also added to the input layer of the GA-BP neural network, and two neural network models with 5-7-1 structure are established. To distinguish these two five-factor models, the model with $size$ was named as the five-factor-1 model, and its structure is shown in Figure 7b. The model with v_n was named as five-factor-2 model, and its structure is shown in Figure 7c. Comparing the prediction results of the two models would be essential in order to observe whether there are factors that have a more significant impact on peak shear strength.

It can be seen from Table 3 that all these six factors have a significant effect on peak shear strength, thus a 6-7-1 structure model was established using these six factors as input factors as shown in Figure 7d. The prediction results of the six-factor model are compared with the prediction results of the model containing four factors and five factors to observe whether increasing the number of input factors can improve the prediction accuracy of the GA-BP neural network.

The constructed neural network model can be expressed in the form of functions. After training, the connection weights and thresholds of the hidden layer and output layer of the model are obtained as shown in Appendix B.

3.3. Forecasting Results

After determining the structure, the GA-BP neural network is trained under the optimization of a genetic algorithm. The R^2 , MAE , MBE , and $RMSE$ of the training results of each neural network model are shown in Table 5. At the same time, Table 5 also shows the prediction results of the BP neural network without genetic algorithm optimization. It can be seen that the neural network model optimized by genetic algorithm is better. It can be seen from Table 5 that the R^2 of each GA-BP neural network model is above 0.93, and the R^2 of the six-factor training set reaches 0.96, indicating that the trained model with more input factors has a better prediction accuracy. Using Tables 4 and 5 for comparison, the indicators of each GA-BP neural network model are basically better than the JRC-JCS model.

Table 5. Training results of neural network models.

		Factors	GA-BP four-factor model	GA-BP five-factor-1 model	GA-BP five-factor-2 model	GA-BP six-factor model
Training set	R^2		0.94	0.95	0.95	0.96
	MAE		0.21	0.20	0.21	0.17
	MBE		0.04	0.01	0.00	0.01
	$RMSE$		0.31	0.28	0.28	0.24
Test set	R^2		0.93	0.93	0.95	0.93
	MAE		0.22	0.23	0.17	0.23
	MBE		0.14	0.04	−0.02	0.06
	$RMSE$		0.31	0.33	0.24	0.37
		Factors	BP four-factor model	BP five-factor-1 model	BP five-factor-2 model	BP six-factor model
Training set	R^2		0.92	0.92	0.94	0.94
	MAE		0.24	0.26	0.24	0.22
	MBE		−0.01	−0.09	0.03	−0.01
	$RMSE$		0.33	0.34	0.31	0.27
Test set	R^2		0.90	0.92	0.93	0.94
	MAE		0.36	0.25	0.25	0.29
	MBE		−0.04	0.34	0.11	−0.05
	$RMSE$		0.47	0.33	0.32	0.36

In addition to observing MAE , MBE , $RMSE$, the prediction accuracy of the GA-BP neural network can be observed by linear fitting of real value and predicted value. As shown in Figure 8, the linear fitting plots of real value and predicted value of training set and test set in each model are drawn. It can be seen from Figure 8 that the fitting lines of the real value and the predicted value are very close to $y = x$, and R^2 is above 0.9. As the number of input factors increases, the R^2 of the training set also increases.

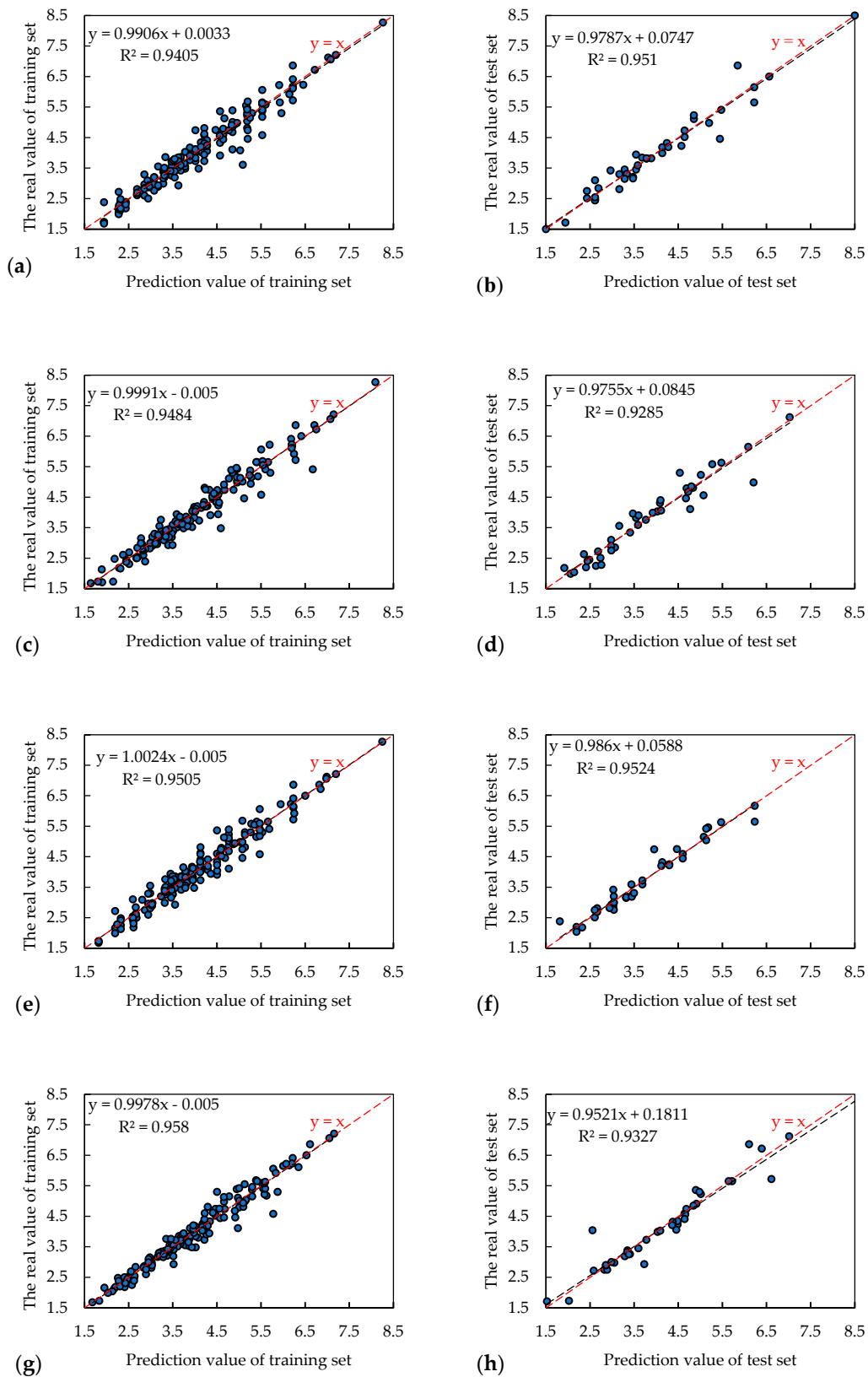


Figure 8. Linear fitting of real value and predicted value: (a) four-factor model training set; (b) four-factor model test set; (c) five-factor-1 model training set; (d) five-factor-1 model test set; (e) five-factor-2 model training set; (f) five-factor-2 model test set; (g) six-factor model training set; (h) six-factor model test set.

4. Error Analysis

The JRC-JCS model and four GA-BP neural network models were used to predict 205 sets of data. The prediction results are shown in Figure 9.

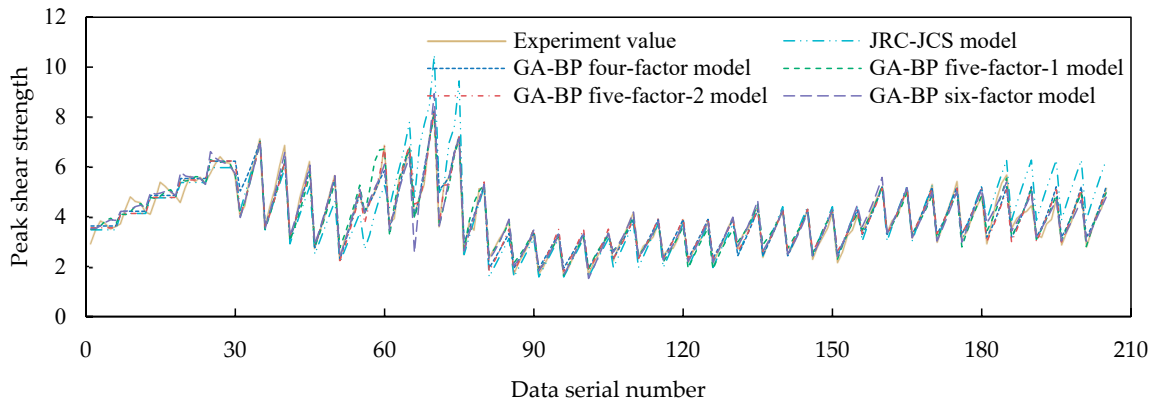


Figure 9. Comparison diagram of peak shear strength prediction of each factor.

In datasets 0 to 30, the prediction trend of the JRC-JCS model, GA-BP four-factor model and GA-BP five-factor-2 model is very similar, which shows that the JRC-JCS model can well predict the relationship between σ_n , φ , JRC, JCS and peak shear strength. The trend of peak shear strength predicted by each model is roughly the same as that of the experimental value. However, the JRC-JCS model has obvious over-predicted values between datasets 60 to 80 and between datasets 180 to 205. Compared with other GA-BP neural networks, the prediction results of the four-factor model between datasets 60 and 80 are also slightly higher than other models. The normal stress range between datasets 60~80 is 3~7 MPa, and the normal stress range of the remaining datasets is 2~4 MPa. The normal stress value of datasets 60~80 is higher. The roughness coefficient of rock joints in datasets 180~205 is 17, and the roughness coefficient of other datasets is generally less than 17. Because the neural network model contains many factors, the sensitivity of the JRC-JCS model to the joint surface roughness and the applied normal stress is more obvious than other models, so the predicted value is higher when the normal stress and roughness are larger. Formula (25) is used to calculate the error of the prediction results of these five models, and the calculation results are shown in Table 6.

$$error = \frac{1}{n} \sum_{i=1}^n \left| \frac{\tau_t - \tau_p}{\tau_t} \right| \times 100\% \tag{25}$$

where n is the number of prediction data; τ_t is the experimental value; τ_p is predicted value.

Table 6. Errors of each model.

Model	JRC-JCS Model	GA-BP Four-Factor Model	GA-BP Five-Factor-1 Model	GA-BP Five-Factor-2 Model	GA-BP Six-Factor Model
error	11.2%	5.7%	5.4%	5.4%	4.6%

The error of each set of data is shown in Figure 10. It can be seen from Table 5 and Figure 8 that the error of the JRC-JCS model fluctuates greatly, up to nearly 50%, and the average absolute error is 11.21%. The error of the GA-BP neural network model is relatively small. In the four GA-BP neural network models, with the increase of model factors, the average absolute error shows a significant downward trend. In the model with two input layers of five factors, the average absolute error of the model with v_n is less than the average absolute error of the model with $size$. Combined with the correlation analysis in Table 6, the

correlation coefficient between the v_n and the peak shear strength is higher than the *size* and the peak shear strength; the higher the correlation between the input factors and the output results of the GA-BP neural network, the better the prediction accuracy of the model.

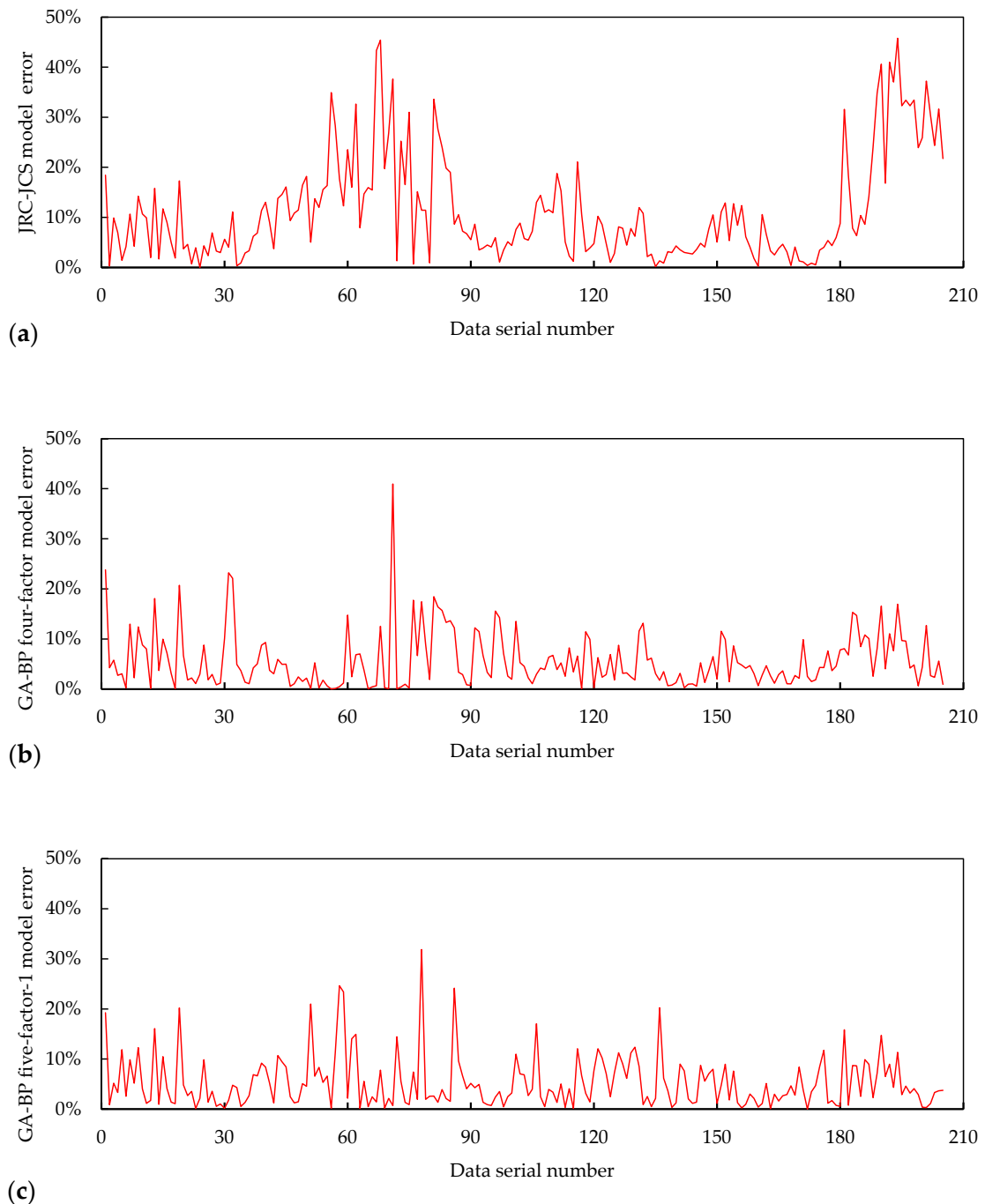
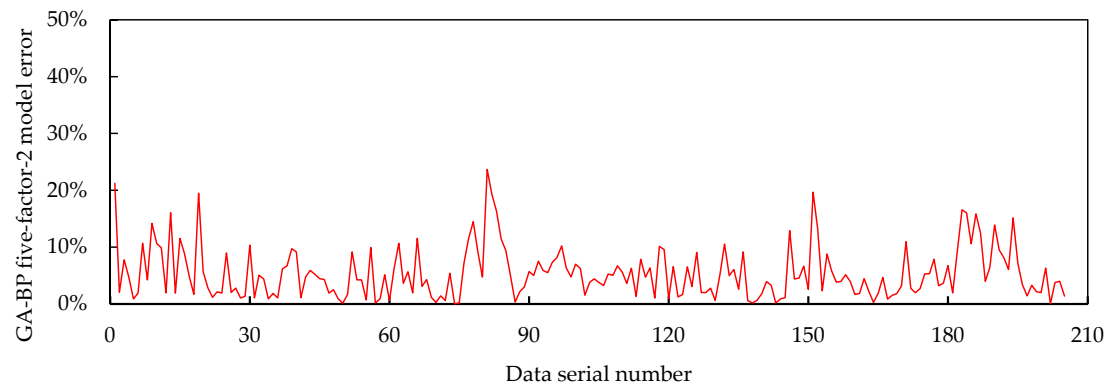
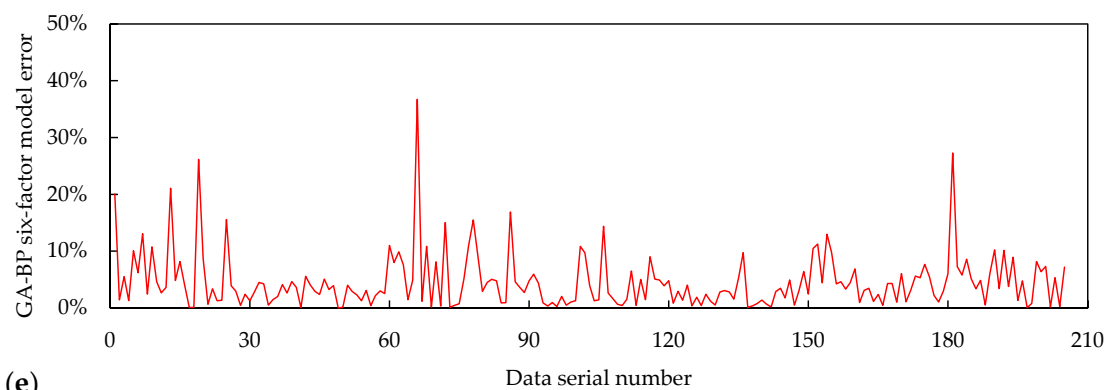


Figure 10. Cont.



(d)



(e)

Figure 10. The error diagram of prediction results of each model: (a) JRC-JCS model error; (b) GA-BP four-factor model error; (c) GA-BP five-factor-1 model error; (d) GA-BP five-factor-2 model error; (e) GA-BP six-factor model error.

5. Discussion

The peak shear strength of rock joints has an important influence on the safety and stability of rock mass engineering. Accurate prediction of the peak shear strength of rock joints plays an important role in the stability evaluation of rock mass. Higher predicted shear strength than its true value is dangerous. Lower predicted shear strength than its true value will cause waste of resources. Therefore, this paper establishes some neural network models to predict the peak shear strength of rock joints accurately. Because the geometric characteristics of the joint itself have certain randomness, and the contact relationship at the joint is more complex, sometimes there will be a local embedding phenomenon, resulting in differences in shear strength, so it is inevitable that there will be some differences in the individual prediction results. There are deviations in the accurate definition of some factors, and the results obtained by using different methods to process some factors will be different. At the same time, there are some factors of the material itself that have an objective effect on the peak shear strength, such as temperature, water content, rock type, etc., which can also be used as input factors to improve the accuracy of the neural network model in future work.

6. Conclusions

This paper collects data from three different direct shear tests. When roughness is processed, three experiments use three methods to estimate the roughness. When the joint compressive strength is processed, the test of the two-body interface is included, and the JCS_a and JCS_b of the two-body interface are converted into JCS_{ab} according to the sharing coefficient. A GA-BP four-factor model was established by using σ_n , JRC , JCS , φ ; the GA-BP

five-factor-1 model was established by using $\sigma_n, JRC, JCS, \varphi, size$; the GA-BP five-factor-2 model was established by using $\sigma_n, JRC, JCS, \varphi, v_n$; and a GA-BP six-factor model was established by using $\sigma_n, JRC, JCS, \varphi, size, v_n$. According to the number of different factors or the type of factors, the model with the best prediction effect was determined. The main conclusions are the following:

(1) The peak shear strength of the rock joint is highly correlated with normal stress and roughness of the rock joint. The peak shear strength of rock joints can be improved by enhancing normal stress or increasing roughness.

(2) A BP neural network optimized by genetic algorithm can effectively predict the shear mechanical properties of jointed rock. The average error of multi-factor prediction was controlled at 4.5%. The quantitative mapping relationship between rock factors and peak shear strength was constructed, and an intelligent prediction method of peak shear strength of rock was formed.

(3) The higher the correlation between the input factors and the output results of the GA-BP neural network, the greater the relevance of the input factors, and the better the prediction accuracy of the model.

In this paper, a GA-BP neural network is applied to the prediction of joint shear strength, and this idea is novel. Compared with the JRC-JCS model, the GA-BP neural network model has better prediction accuracy in all aspects. Among the four GA-BP neural network models, the six-factor model is better. Due to the limitations of the data, no factors such as shear rate were added to the input layer, and no more rock types were input. Adding more influencing factors to the GA-BP neural network model and increasing the range of data can improve the accuracy of prediction to a greater extent, which will be the goal of future work.

Author Contributions: Methodology, H.L.; validation, A.S.; data curation, Z.Z.; writing—original draft preparation, C.Z.; writing—review and editing, B.G. Formal analysis, P.Z. All authors have read and agreed to the published version of the manuscript.

Funding: This research received no external funding.

Institutional Review Board Statement: The study did not require ethical approval.

Informed Consent Statement: Not applicable.

Data Availability Statement: No new data were created or analyzed in this study.

Conflicts of Interest: The authors declare no conflict of interest.

Appendix A

Table A1. Data of $\sigma_n, JRC, JCS, size, v_n$ and τ_t .

Number	σ_n	JRC	JCS	φ	Size	V_n	τ_t	Number	σ_n	JRC	JCS	φ	Size	V_n	τ_t
1	2	12.88	65.69	40.51	2500	2	2.93	104	3.5	1	65.69	36.8	9025	1	2.9
2	2	12.88	65.69	40.51	3600	2	3.48	105	4	1	65.69	36.8	9025	1	3.37
3	2	12.88	65.69	40.51	4900	2	3.85	106	2	5	65.69	36.8	1225	1	2.25
4	2	12.88	65.69	40.51	6400	2	3.73	107	2.5	5	65.69	36.8	1225	1	2.81
5	2	12.88	65.69	40.51	8100	2	3.52	108	3	5	65.69	36.8	1225	1	3.2
6	2	12.88	65.69	40.51	10,000	2	3.62	109	3.5	5	65.69	36.8	1225	1	3.71
7	2.5	12.88	65.69	40.51	2500	2	3.73	110	4	5	65.69	36.8	1225	1	4.17
8	2.5	12.88	65.69	40.51	3600	2	4.31	111	2	5	65.69	36.8	2500	1	2.41
9	2.5	12.88	65.69	40.51	4900	2	4.81	112	2.5	5	65.69	36.8	2500	1	2.84
10	2.5	12.88	65.69	40.51	6400	2	4.62	113	3	5	65.69	36.8	2500	1	3
11	2.5	12.88	65.69	40.51	8100	2	4.58	114	3.5	5	65.69	36.8	2500	1	3.21
12	2.5	12.88	65.69	40.51	10,000	2	4.21	115	4	5	65.69	36.8	2500	1	3.76
13	3	12.88	65.69	40.51	2500	2	4.11	116	2	5	65.69	36.8	4225	1	2.48
14	3	12.88	65.69	40.51	3600	2	4.68	117	2.5	5	65.69	36.8	4225	1	2.69
15	3	12.88	65.69	40.51	4900	2	5.39	118	3	5	65.69	36.8	4225	1	2.76

Table A1. Cont.

Number	σ_n	JRC	JCS	φ	Size	V_n	τ_t	Number	σ_n	JRC	JCS	φ	Size	V_n	τ_t
16	3	12.88	65.69	40.51	6400	2	5.23	119	3.5	5	65.69	36.8	4225	1	3.16
17	3	12.88	65.69	40.51	8100	2	5.01	120	4	5	65.69	36.8	4225	1	3.9
18	3	12.88	65.69	40.51	10,000	2	4.85	121	2	5	65.69	36.8	6400	1	2.18
19	3.5	12.88	65.69	40.51	2500	2	4.58	122	2.5	5	65.69	36.8	6400	1	2.63
20	3.5	12.88	65.69	40.51	3600	2	5.18	123	3	5	65.69	36.8	6400	1	2.99
21	3.5	12.88	65.69	40.51	4900	2	5.63	124	3.5	5	65.69	36.8	6400	1	3.25
22	3.5	12.88	65.69	40.51	6400	2	5.41	125	4	5	65.69	36.8	6400	1	3.82
23	3.5	12.88	65.69	40.51	8100	2	5.59	126	2	5	65.69	36.8	9025	1	2.13
24	3.5	12.88	65.69	40.51	10,000	2	5.37	127	2.5	5	65.69	36.8	9025	1	2.61
25	4	12.88	65.69	40.51	2500	2	5.72	128	3	5	65.69	36.8	9025	1	2.98
26	4	12.88	65.69	40.51	3600	2	6.11	129	3.5	5	65.69	36.8	9025	1	3.56
27	4	12.88	65.69	40.51	4900	2	6.41	130	4	5	65.69	36.8	9025	1	3.96
28	4	12.88	65.69	40.51	6400	2	6.17	131	2	9	65.69	36.8	1225	1	2.75
29	4	12.88	65.69	40.51	8100	2	6.15	132	2.5	9	65.69	36.8	1225	1	3.29
30	4	12.88	65.69	40.51	10,000	2	5.65	133	3	9	65.69	36.8	1225	1	3.51
31	2	16	65.69	40.51	2500	2	4.08	134	3.5	9	65.69	36.8	1225	1	4.03
32	2.5	16	65.69	40.51	2500	2	4.46	135	4	9	65.69	36.8	1225	1	4.41
33	3	16	65.69	40.51	2500	2	5.65	136	2	9	65.69	36.8	2500	1	2.39
34	3.5	16	65.69	40.51	2500	2	6.23	137	2.5	9	65.69	36.8	2500	1	2.96
35	4	16	65.69	40.51	2500	2	7.12	138	3	9	65.69	36.8	2500	1	3.33
36	2	12.88	65.69	40.51	2500	2	3.59	139	3.5	9	65.69	36.8	2500	1	3.81
37	2.5	12.88	65.69	40.51	2500	2	4.4	140	4	9	65.69	36.8	2500	1	4.22
38	3	12.88	65.69	40.51	2500	2	5.11	141	2	9	65.69	36.8	4225	1	2.51
39	3.5	12.88	65.69	40.51	2500	2	6.06	142	2.5	9	65.69	36.8	4225	1	2.85
40	4	12.88	65.69	40.51	2500	2	6.86	143	3	9	65.69	36.8	4225	1	3.34
41	2	9.9	65.69	40.51	2500	2	3.2	144	3.5	9	65.69	36.8	4225	1	3.82
42	2.5	9.9	65.69	40.51	2500	2	3.65	145	4	9	65.69	36.8	4225	1	4.25
43	3	9.9	65.69	40.51	2500	2	4.75	146	2	9	65.69	36.8	6400	1	2.31
44	3.5	9.9	65.69	40.51	2500	2	5.46	147	2.5	9	65.69	36.8	6400	1	2.82
45	4	9.9	65.69	40.51	2500	2	6.22	148	3	9	65.69	36.8	6400	1	3.19
46	2	7.09	65.69	40.51	2500	2	2.75	149	3.5	9	65.69	36.8	6400	1	3.55
47	2.5	7.09	65.69	40.51	2500	2	3.41	150	4	9	65.69	36.8	6400	1	4.19
48	3	7.09	65.69	40.51	2500	2	4.04	151	2	9	65.69	36.8	9025	1	2.18
49	3.5	7.09	65.69	40.51	2500	2	4.91	152	2.5	9	65.69	36.8	9025	1	2.6
50	4	7.09	65.69	40.51	2500	2	5.65	153	3	9	65.69	36.8	9025	1	3.26
51	2	4.46	65.69	40.51	2500	2	2.28	154	3.5	9	65.69	36.8	9025	1	3.48
52	2.5	4.46	65.69	40.51	2500	2	3.09	155	4	9	65.69	36.8	9025	1	4.06
53	3	4.46	65.69	40.51	2500	2	3.59	156	2	13	65.69	36.8	1225	1	3.45
54	3.5	4.46	65.69	40.51	2500	2	4.32	157	2.5	13	65.69	36.8	1225	1	3.84
55	4	4.46	65.69	40.51	2500	2	4.94	158	3	13	65.69	36.8	1225	1	4.34
56	3	13.54	16.12	32.11	1962.5	1	4.15	159	3.5	13	65.69	36.8	1225	1	4.79
57	4	11.8	16.12	32.11	1962.5	1	4.56	160	4	13	65.69	36.8	1225	1	5.22
58	5	14.22	16.12	32.11	1962.5	1	4.98	161	2	13	65.69	36.8	2500	1	3.38
59	6	14.52	16.12	32.11	1962.5	1	5.41	162	2.5	13	65.69	36.8	2500	1	3.86
60	7	13.12	16.12	32.11	1962.5	1	6.86	163	3	13	65.69	36.8	2500	1	4.03
61	3	19	31.82	36	1962.5	1	3.76	164	3.5	13	65.69	36.8	2500	1	4.59
62	4	18.4	31.82	36	1962.5	1	3.94	165	4	13	65.69	36.8	2500	1	5.04
63	5	17.61	31.82	36	1962.5	1	5.55	166	2	13	65.69	36.8	4225	1	3.17
64	6	17.29	31.82	36	1962.5	1	5.92	167	2.5	13	65.69	36.8	4225	1	3.72
65	7	18.35	31.82	36	1962.5	1	6.72	168	3	13	65.69	36.8	4225	1	4.18
66	3	9.06	36.84	47.39	1962.5	1	4.04	169	3.5	13	65.69	36.8	4225	1	4.52
67	4	12.57	36.84	47.39	1962.5	1	4.74	170	4	13	65.69	36.8	4225	1	5.3
68	5	11.11	36.84	47.39	1962.5	1	5.3	171	2	13	65.69	36.8	6400	1	2.99
69	6	9.19	36.84	47.39	1962.5	1	7.06	172	2.5	13	65.69	36.8	6400	1	3.59
70	7	12.33	36.84	47.39	1962.5	1	8.27	173	3	13	65.69	36.8	6400	1	4.2
71	3	18.13	21.15	43.5	1962.5	1	3.61	174	3.5	13	65.69	36.8	6400	1	4.73
72	4	13.57	21.15	43.5	1962.5	1	5.3	175	4	13	65.69	36.8	6400	1	5.42
73	5	17.43	21.15	43.5	1962.5	1	5.58	176	2	13	65.69	36.8	9025	1	3.15

Table A1. Cont.

Number	σ_n	JRC	JCS	φ	Size	V_n	τ_t	Number	σ_n	JRC	JCS	φ	Size	V_n	τ_t
74	6	14.84	21.15	43.5	1962.5	1	6.5	177	2.5	13	65.69	36.8	9025	1	3.42
75	7	20.73	21.15	43.5	1962.5	1	7.21	178	3	13	65.69	36.8	9025	1	3.99
76	3	8.21	8.52	35.89	1962.5	1	2.5	179	3.5	13	65.69	36.8	9025	1	4.44
77	4	8.21	8.52	35.89	1962.5	1	3.76	180	4	13	65.69	36.8	9025	1	4.81
78	5	8.21	8.52	35.89	1962.5	1	3.48	181	2	17	65.69	36.8	1225	1	2.93
79	6	8.21	8.52	35.89	1962.5	1	5.13	182	2.5	17	65.69	36.8	1225	1	3.8
80	7	8.21	8.52	35.89	1962.5	1	5.15	183	3	17	65.69	36.8	1225	1	4.74
81	2	1	65.69	36.8	1225	1	2.38	184	3.5	17	65.69	36.8	1225	1	5.36
82	2.5	1	65.69	36.8	1225	1	2.72	185	4	17	65.69	36.8	1225	1	5.68
83	3	1	65.69	36.8	1225	1	3.1	186	2	17	65.69	36.8	2500	1	3.55
84	3.5	1	65.69	36.8	1225	1	3.42	187	2.5	17	65.69	36.8	2500	1	3.94
85	4	1	65.69	36.8	1225	1	3.86	188	3	17	65.69	36.8	2500	1	4.12
86	2	1	65.69	36.8	2500	1	1.73	189	3.5	17	65.69	36.8	2500	1	4.23
87	2.5	1	65.69	36.8	2500	1	2.2	190	4	17	65.69	36.8	2500	1	4.46
88	3	1	65.69	36.8	2500	1	2.54	191	2	17	65.69	36.8	4225	1	3.3
89	3.5	1	65.69	36.8	2500	1	2.94	192	2.5	17	65.69	36.8	4225	1	3.19
90	4	1	65.69	36.8	2500	1	3.31	193	3	17	65.69	36.8	4225	1	3.73
91	2	1	65.69	36.8	4225	1	1.73	194	3.5	17	65.69	36.8	4225	1	3.91
92	2.5	1	65.69	36.8	4225	1	2.04	195	4	17	65.69	36.8	4225	1	4.74
93	3	1	65.69	36.8	4225	1	2.45	196	2	17	65.69	36.8	6400	1	2.89
94	3.5	1	65.69	36.8	4225	1	2.87	197	2.5	17	65.69	36.8	6400	1	3.4
95	4	1	65.69	36.8	4225	1	3.26	198	3	17	65.69	36.8	6400	1	3.83
96	2	1	65.69	36.8	6400	1	1.68	199	3.5	17	65.69	36.8	6400	1	4.6
97	2.5	1	65.69	36.8	6400	1	1.99	200	4	17	65.69	36.8	6400	1	4.98
98	3	1	65.69	36.8	6400	1	2.44	201	2	17	65.69	36.8	9025	1	2.81
99	3.5	1	65.69	36.8	6400	1	2.89	202	2.5	17	65.69	36.8	9025	1	3.45
100	4	1	65.69	36.8	6400	1	3.27	203	3	17	65.69	36.8	9025	1	4.11
101	2	1	65.69	36.8	9025	1	1.71	204	3.5	17	65.69	36.8	9025	1	4.33
102	2.5	1	65.69	36.8	9025	1	2.16	205	4	17	65.69	36.8	9025	1	5.15
103	3	1	65.69	36.8	9025	1	2.5								

Appendix B

The specific expression of the four-factor model is as follows:

$$\tau_p = f_{GA-BP}(\sigma_n, JRC, JCS, \varphi) \tag{A1}$$

Input to the hidden layer weights $w_{7 \times 4} =$

$$\begin{bmatrix} 0.78238797 & 0.006151265 & 0.559252414 & -0.022988896 \\ 0.12224167 & 0.699814191 & 0.145962199 & 0.110511176 \\ -0.444862767 & 0.038327763 & -0.64180243 & -0.659542444 \\ 0.281185003 & -0.965904934 & -0.614938516 & 0.585583209 \\ 0.86086054 & 0.155272565 & 0.297204638 & 0.980305703 \\ -0.725286337 & 0.217959521 & 0.177400843 & 0.916072863 \\ -0.153793465 & -0.568055925 & 0.770665435 & 0.496058452 \end{bmatrix}$$

Hidden layer threshold $b_{7 \times 1}^T =$

$$[0.823406449 \quad -0.421283472 \quad -0.495875986 \quad -0.168409719 \quad 0.542302059 \quad 0.53883313 \quad 0.180495919]$$

Weight from hidden layer to output layer $w_{1 \times 7} =$

$$[0.594569848 \quad -0.304958592 \quad -0.738011295 \quad -0.96820142 \quad -0.314689617 \quad 0.403932703 \quad 0.673183979]$$

Output layer threshold $b_{1 \times 1} =$

$$[0.26553184]$$

The specific expression of the five-factor-1 model is as follows:

$$\tau_p = f_{GA-BP}(\sigma_n, JRC, JCS, \varphi, Size) \tag{A2}$$

Input to the hidden layer weights $w_{7 \times 5} =$

$$\begin{bmatrix} 0.667155213 & -0.655870612 & 0.248106939 & -0.189063966 & -0.063270789 \\ 0.482987934 & -0.088293321 & 0.441802043 & 0.314950534 & -0.602822908 \\ 0.481731069 & 0.506868286 & -0.014792291 & 0.259463730 & -0.497285292 \\ -0.428939292 & 0.686079351 & 0.108863950 & 0.552253051 & -0.893309452 \\ -0.431134193 & 0.856826414 & 0.201418130 & -0.304624571 & -0.459542985 \\ -0.619490698 & -0.203589947 & -0.448510158 & 0.311206112 & 0.427356204 \\ 0.282766515 & 0.313212628 & -0.264193033 & -0.348119603 & 0.061254327 \end{bmatrix}$$

Hidden layer threshold $b_{7 \times 1}^T =$

$$[-0.217903171 \quad 0.333022423 \quad -0.159279128 \quad 0.82777986 \quad -0.165355843 \quad -0.639250519 \quad -0.108405099]$$

Weight from hidden layer to output layer $w_{1 \times 7} =$

$$[0.551944259 \quad 0.04486292 \quad 0.096930339 \quad 0.207360829 \quad 0.583442549 \quad -0.42827962 \quad -0.237057586]$$

Output layer threshold $b_{1 \times 1} =$

$$[0.786505588]$$

The specific expression of the five-factor-2 model is as follows:

$$\tau_p = f_{GA-BP}(\sigma_n, JRC, JCS, \varphi, v_n) \tag{A3}$$

Input to the hidden layer weights $w_{7 \times 5} =$

$$\begin{bmatrix} 0.273047256 & 0.305717466 & -0.599473941 & -0.557541506 & 0.070028479 \\ 0.540056814 & -0.631012617 & 0.271568874 & -0.522003598 & -0.105043307 \\ 0.25716471 & 0.276752509 & 0.551193534 & 0.193336208 & -0.678159167 \\ 0.220523739 & 0.028366 & 0.482615828 & 0.86886645 & 0.317527661 \\ -0.250524856 & 0.530794807 & 0.812125895 & -0.402229147 & -0.506802879 \\ -0.451378505 & -0.226523067 & 0.223087738 & 0.536325541 & 0.220742544 \\ 0.013291297 & -0.247780736 & -0.299314983 & 0.041163144 & 0.573582139 \end{bmatrix}$$

Hidden layer threshold $b_{7 \times 1}^T =$

$$[-0.142483411 \quad 0.033067931 \quad 0.434268109 \quad 0.529580502 \quad -0.11789349 \quad 0.271972823 \quad -0.6347275]$$

Weight from hidden layer to output layer $w_{1 \times 7} =$

$$[0.277483091 \quad 0.000535253 \quad -0.363035577 \quad -0.471799881 \quad -0.465165465 \quad -0.394055314 \quad 0.658825554]$$

Output layer threshold $b_{1 \times 1} =$

$$[0.217788332]$$

The specific expression of the six-factor model is as follows:

$$\tau_p = f_{GA-BP}(\sigma_n, JRC, JCS, \varphi, Size, v_n) \tag{A4}$$

Input to the hidden layer weights $w_{7 \times 6} =$

$$\begin{bmatrix} -0.433322223 & 0.429946865 & 0.424252082 & 0.703113658 & 0.660662443 & 0.287477619 \\ 0.574445196 & 0.051094972 & 0.455487299 & -0.149100734 & 0.352446035 & 0.212017079 \\ -0.359464603 & 0.111925361 & -0.207397903 & 0.266439922 & 0.415585492 & 0.40214093 \\ -0.169409187 & -0.120843582 & -0.015508303 & -0.005962941 & 0.023787119 & -0.557586803 \\ -0.127837976 & -0.072352899 & 0.408400737 & -0.016568927 & 0.080544553 & 0.272602714 \\ -0.202478508 & 0.048918596 & 0.223988037 & -0.178112945 & -0.137026824 & -0.649940369 \\ 0.07514333 & 0.363434317 & -0.398613355 & 0.782172748 & -0.001317362 & 0.142845959 \end{bmatrix}$$

Hidden layer threshold $b_{7 \times 1}^T =$

$$\begin{bmatrix} 0.31812295 & -0.653098785 & 0.192202639 & -0.190265294 & -0.055570417 & 0.725822551 & 0.184984033 \end{bmatrix}$$

Weight from hidden layer to output layer $w_{1 \times 7} =$

$$\begin{bmatrix} -0.036943679 & -0.304669461 & -0.001007669 & 0.461609068 & -0.329812939 & 0.467953947 & 0.270241955 \end{bmatrix}$$

Output layer threshold $b_{1 \times 1} =$

$$\begin{bmatrix} 0.181067327 \end{bmatrix}$$

References

- Barton, N. Review of a new shear-strength criterion for rock joints. *Eng. Geol.* **1973**, *7*, 287–332. [CrossRef]
- Heuze, F.E. Scale effects in the determination of rock mass strength and deformability. *Rock Mech.* **1980**, *12*, 167–192. [CrossRef]
- Zhang, X.B.; Yi, B.; Jiang, Q.H.; Feng, X.X.; Chen, N. Evaluation Models for the Peak Shear-Strength and Shear-Resistance Components of Rough Rock Joints. *ASTM Int. J. Test. Eval.* **2017**, *45*, 2128–2138. [CrossRef]
- Liu, X.; Deng, Z.; Liu, Y.; Liu, S.; Lu, Y.; Han, Y. An experimental study on the cumulative damage and shear properties of rock joints under pre-peak cyclic shear loading. *Chin. J. Rock Mech. Eng.* **2018**, *37*, 2664–2675. [CrossRef]
- Yong, R.; Ye, J.; Liang, Q.F.; Huang, M.; Du, S.G. Estimation of the joint roughness coefficient (JRC) of rock joints by vector similarity measures. *Bull. Eng. Geol. Environ.* **2018**, *77*, 735–749. [CrossRef]
- Ban, L.; Du, W.; Qi, C.; Zhu, C. Modified 2D roughness parameters for rock joints at two different scales and their correlation with JRC. *Int. J. Rock Mech. Min. Sci.* **2021**, *137*, 104549. [CrossRef]
- Ma, X.; Yu, J.; Wang, F. Experimental study on shear behavior of rock under uniform distribute normal stress. In Proceedings of the 2022 Industrial Architecture Academic Exchange Conference, Beijing, China, 14 October 2022. Available online: https://kns.cnki.net/kcms2/article/abstract?v=ZoyQtr8ALTd4yt00o7lckRNHvq-GdAyXnIvoEkU8bi_XIEHgxPFkgk9JNivPP_em0I8Zw5IE_CY-TdRsG74LbiqL3ewZXLX2NT2GNU6tRmXk7vT89fQreJdsOEGRIbhVniHyF4KwBX1ZqqJYdFAQatsQDfvymYsqFj8XPN3oZiCb_xaQ9SvC0xa1QnmGRN7qWcpXzRqUdkyC5BrftgfjGqVjnHAXQt2&uniplatform=NZKPT (accessed on 17 October 2024).
- Liu, J.; Guo, B.; Cheng, T.; Sun, J.; Tian, S.; Chen, Y. Experimental study on empirical formula of peak shear strength for rock-concrete interface. *Chin. J. Rock Mech. Eng.* **2023**, *42*, 2552–2565. [CrossRef]
- Barton, N.; Wang, C.; Yong, R. Advances in joint roughness coefficient (JRC) and its engineering applications. *J. Rock Mech. Geotech. Eng.* **2023**, *15*, 3352–3379. [CrossRef]
- Grasselli, G.; Egger, P.; Wirth, J.; Hopkins, D. Characterization of the parameters that govern the peak shear strength rock joints. In Proceedings of the 38th U.S. Symposium on Rock Mechanics (USRMS), Washington, DC, USA, 7–10 July 2001; ARMA: Richardson, TX, USA, 2001; pp. 1–817.
- Shen, M.R.; Zhang, Q.Z. Experimental Study of Shear Deformation Characteristics of Rock Mass Discontinuities. *Chin. J. Rock Mech. Eng.* **2010**, *29*, 713–719.
- Chen, S.; Zhu, W.; Wang, C.; Wang, C.; Guo, L. Peak Shear Strength of 3D Rock Discontinuities Based on Anisotropic Properties. *Chin. J. Rock Mech. Eng.* **2016**, *35*, 2013–2021. [CrossRef]
- Yang, J.; Rong, G.; Hou, D.; Peng, J.; Zhou, C. Experimental Study on Peak Shear Strength Criterion for Rock Joints. *Rock Mech. Rock Eng.* **2016**, *49*, 821–835. [CrossRef]
- Dong, Y. Experimental Study on Mechanical Shear Properties of Irregular Rock Fractures. Master's Thesis, Henan Polytechnic University, Jiaozuo, China, 2017.
- Tian, Y.; Liu, Q.; Liu, D.; Kang, Y.; Deng, P.; He, F. Updates to Grasselli's Peak Shear Strength Model. *Rock Mech. Rock Eng.* **2018**, *51*, 2115–2133. [CrossRef]
- Liu, Q.; Tian, Y.; Ji, P.; Ma, H. Experimental Investigation of the Peak Shear Strength Criterion Based on Three-Dimensional Surface Description. *Rock Mech. Rock Eng.* **2018**, *51*, 1005–1025. [CrossRef]
- Wang, S.; Yin, H.; Zhang, Z.; Wei, W. A new prediction model for peak shear strength of rock joints considering the 3d morphology parameters. *J. Northeast. Univ. (Nat. Sci.)* **2021**, *42*, 1609. [CrossRef]

18. Sheng, J.; Xu, L.; Zhou, X.; Peng, Z. Research on Peak Shear Strength Model of Rock Joints Based on Three-Dimensional Shape Parameters. *Metal Mine* **2022**, *6*, 9–16. [[CrossRef](#)]
19. Cheng, T.; Guo, B.; Sun, J. A strength empirical formula of irregular rock joints based on peak shear test. *Chin. J. Rock Mech. Eng.* **2022**, *41*, 93–105. [[CrossRef](#)]
20. Wu, Q.; Xu, Y.; Tang, H.; Fang, K.; Jiang, Y.; Liu, C.; Wang, X. Peak Shear Strength Prediction for Discontinuities Between Two Different Rock Types Using a Neural Network Approach. *Bull. Eng. Geol. Environ.* **2019**, *78*, 2315–2329. [[CrossRef](#)]
21. Huang, M.; Hong, C.; Chen, J.; Ma, C.; Li, C.; Huang, Y. Prediction of Peak Shear Strength of Rock Joints Based on Back-Propagation Neural Network. *Int. J. Geomech.* **2021**, *21*, 4021085. [[CrossRef](#)]
22. Wang, W. Study on Prediction of Shear Mechanics Characteristics of Rock Joints Based on BP Neural Network. Master's Thesis, Dalian University of Technology, Dalian, China, 2021. [[CrossRef](#)]
23. Shen, H.; Liu, Y.; Li, H.; Xia, X.; Liu, B.; Yu, C. Prediction of Peak Shear Strength of Joints Based on Machine Learning Algorithms. In Proceedings of the 2022 3rd International Conference on Computer Vision, Image and Deep Learning & International Conference on Computer Engineering and Applications (CVIDL & ICCEA), Changchun, China, 20–22 May 2022; pp. 821–824. [[CrossRef](#)]
24. Lin, Y.; Wang, H.; Wei, L.; Xu, J.; Ma, H. Analysis of Mechanical Properties of Fractured Rock Mechanics and Intelligent Prediction Method Considering Joint Morphology Characteristics. Yangtze River. 2023. Available online: https://kns.cnki.net/kcms2/article/abstract?v=ZoyQtr8ALTdMPmtskJnKr-ycn8nAzLcYc5HISwVFm7Wa9JR9HwpXOOpdDpHG6CXgzgKUP48_o9AmHYFQDcKyk3jec-B1Jj1NygOETUHsInsNaIfTaqIBvrQBS8CqiOCe0AwNphEOZT8RyTtjijolcrf3V-3zueaECg49DSA6Vsw_hMt33mAvAfU5wV3qTLPC&uniplatform=NZKPT&language=CHS (accessed on 17 October 2024).
25. Liu, Z.; Li, D.; Liu, Y.; Yang, B.; Zhang, Z. Prediction of Uniaxial Compressive Strength of Rock Based on Lithology Using Stacking Models. *Rock Mech. Bull.* **2023**, *2*, 100081. [[CrossRef](#)]
26. Wei, X.; Shahani, N.M.; Zheng, X. Predictive Modeling of the Uniaxial Compressive Strength of Rocks Using an Artificial Neural Network Approach. *Mathematics* **2023**, *11*, 1650. [[CrossRef](#)]
27. He, M.; Zhang, Z.; Ren, J.; Huan, J.; Li, G.; Chen, Y.; Li, N. Deep convolutional neural network for fast determination of the rock strength parameters using drilling data. *Int. J. Rock Mech. Min. Sci.* **2019**, *123*, 104084. [[CrossRef](#)]
28. Feng, Z.; Hu, X.; Tian, Z.; Jiang, B.; Zhang, H.; Zhang, W. Bi-LSTM-Based Dynamic Prediction Model for Pulling Speed of Czochralski Single-Crystal Furnace. *J. Comput. Inf. Sci. Eng.* **2023**, *23*, 041010. [[CrossRef](#)]
29. Chen, J.; Zhao, Z.; Zhang, J. Predicting peak shear strength of rock fractures using tree-based models and convolutional neural network. *Comput. Geotech.* **2024**, *166*, 105965. [[CrossRef](#)]
30. Ma, Z.; Ou, X.; Zhang, B. Development of a convolutional neural network based geomechanical upscaling technique for heterogeneous geological reservoir. *J. Rock Mech. Geotech. Eng.* **2024**, *16*, 2111–2125. [[CrossRef](#)]
31. Xie, H. Fractal Description of Rock Joints. *Chin. J. Rock Mech. Eng.* **1995**, *17*, 18–23.
32. Barton, N.; Choubey, V. The shear strength of rock joints in theory and practice. *Sci. Rock Mech.* **1977**, *10*, 1–54. [[CrossRef](#)]
33. Wang, X.; Yao, Y.; Tao, C.; Chu, D.; Xu, B. Correlation Analysis of Dam Deformation Monitoring Data for Concrete Gravity Dam. *China Rural. Water Hydropower.* **2024**, *8*, 180-187+193.
34. Zhang, Y.; Xu, P.; Lin, J.; Wu, X.; Liu, J.; Xiang, C.; He, Y.; Yang, C.; Xu, C. Earthquake-Triggered Landslide Susceptibility Prediction in Jiuzhaigou Based on BP Neural Network. *J. Eng. Geol.* **2024**, *32*, 133–145. [[CrossRef](#)]
35. Han, B.; Ji, K.; Hu, Y.F.; Yao, S. Application of ANN-PSO-GA Model in UCS Prediction and Mix Proportion Optimization of Wet Shotcrete. *J. Min. Saf. Eng.* **2021**, *38*, 584–591. [[CrossRef](#)]
36. Yan, J.; Zheng, S.; Guo, P.; Zhang, B.; Mao, Z. Prediction of heat transfer characteristics for supercritical co2 based on ga-bp neural network. *CIESC J.* **2021**, *72*, 4649–4657. [[CrossRef](#)]
37. Zhang, X.; Zhang, R.; Chen, X.; Yang, H.; Yu, D.; Song, Y. Strength evolution prediction of concrete structures during long-term service life based on GA-BP neural network. *J. Cent. South Univ. (Sci. Technol.)* **2024**, *55*, 836–850. [[CrossRef](#)]

Disclaimer/Publisher's Note: The statements, opinions and data contained in all publications are solely those of the individual author(s) and contributor(s) and not of MDPI and/or the editor(s). MDPI and/or the editor(s) disclaim responsibility for any injury to people or property resulting from any ideas, methods, instructions or products referred to in the content.